Total harmonic distortion analysis of oxygen reduction reaction in proton exchange membrane fuel cells

Qing Mao [a,b], Ulrike Krewer [a,c,*]

[a] Max Planck Institute for Dynamics of Complex Technical Systems, Sandtorstraße1, 39106 Magdeburg, Germany
[b] Department of Material Science and Chemical Engineering, School of Chemical Engineering, Dalian University of Technology, No. 2, Linggong Road, Dalian 116024, China
[c] Institute of Energy and Process Systems Engineering, TU Braunschweig, Franz-Liszt-Straße 35, 38106 Braunschweig, Germany

ARTICLE INFO

Keywords:
Oxygen reduction reaction (ORR) mechanism
Nonlinear frequency response behavior
Total harmonic distortion (THD) spectroscopy

ABSTRACT

The nonlinear frequency response behavior of a proton exchange membrane fuel cell (PEMFC) with different O_2 stoichiometry is characterized and analyzed by total harmonic distortion (THD) spectroscopy. Damjanovic oxygen reduction reaction (ORR) mechanisms with either oxygen electrochemisorption or oxygen chemisorption are comparatively studied in the simulation through THD spectroscopy and commonly used methods that include steady state current–voltage (*I–V*) curve and electrochemical impedance spectroscopy (EIS). Comparison results show that only THD spectroscopy is able to make a fine distinction for the ORR mechanisms in certain kinetically controlled frequency ranges. The Damjanovic ORR mechanism with oxygen chemisorption is recognized as a better option for the ORR process in the PEMFC due to the reproducible experimental THD spectra. The observed nonlinear response in the frequency range from 2.5 Hz to 15.8 Hz is also recognized as the fingerprint of the ORR process.

1. Introduction

Oxygen reduction reaction (ORR) is one of the most studied electrochemical reactions in modern electrochemistry due to its practical application in fuel cells, metal–air batteries and some other industrial processes [1–5]. In the past decades, considerable progress has been made to understand the ORR process on platinum, platinum-based and non-platinum-based electro-catalysts in either acid or alkaline medium. A large amount of research focuses on the effects of loading, particle size, crystal surfaces as well as alloy materials of the catalyst on the ORR kinetics [6–8]. Moreover, exploring the mechanism and pathway for the ORR process continues to be a challenge due to its complex kinetics. As far as the ORR on platinum in acidic medium is concerned, Damjanovic ORR mechanism has been widely accepted. This conclusion is based on studies of steady state relationships among electrode potential, current density, O_2 partial pressure and pH value of the electrolyte [6,9–11]. For the rate determining step, the step with the first electron transfer was proposed. According to Damjanovic's theory, a mechanism with oxygen electrochemisorption, i.e. active oxygen adsorption:

$$O_2 + Pt + H^+ + e^- \underset{\gamma\cdot d\cdot s}{\overset{K_{101}/K_{102}}{\rightleftharpoons}} PtO_2H_{ads} \quad (1)$$

$$PtO_2H_{ads} + 3H^+ + 3e^- \overset{K_{201}/K_{202}}{\rightleftharpoons} Pt + 2H_2O \quad (2)$$

and one with oxygen chemisorption, i.e. non-active oxygen adsorption:

$$O_2 + Pt \overset{K'_{101}/K'_{102}}{\rightleftharpoons} PtO_{2,ads} \quad (3)$$

$$PtO_{2,ads} + H^+ + e^- \underset{\gamma\cdot d\cdot s}{\overset{K'_{201}/K'_{202}}{\rightleftharpoons}} PtO_2H_{ads} \quad (4)$$

$$PtO_2H_{ads} + 3H^+ + 3e^- \overset{K'_{301}/K'_{302}}{\rightleftharpoons} Pt + 2H_2O \quad (5)$$

are equally feasible to describe the ORR process according to identical steady state current–voltage (*I–V*) relationship [11]. For the later mechanism, the oxygen chemical adsorption step, as shown in Eq. (3), is taken as quasi-equilibrium. When the cathode potential is above 0.8 V, oxygen adsorption is under Temkin conditions;

Abbreviations: CSTR, continuously stirred tank reactor; DMFC, direct methanol fuel cell; EIS, electrochemical impedance spectroscopy; IR, internal resistance; *I–V*, current–voltage; ORR, oxygen reduction reaction; PEMFC, proton exchange membrane fuel cell; SCCM, standard cubic centimeters per minute; THD, total harmonic distortion.

* Corresponding author at: TU Braunschweig, Institute of Energy and Process Systems Engineering, Franz-Liszt-Str. 35, 38106 Braunschweig, Germany.
Tel.: +49 531 391 3030; fax: +49 531 391 5932.
E-mail addresses: u.krewer@tu-bs.de, maoqing@dlut.edu.cn (U. Krewer).

otherwise, it is under Langmuir conditions due to the low oxygen coverage [12].

From above, it is clear that ORR is a complex four-electron transfer reaction that includes a number of elementary steps and reaction intermediates. Each step owns an independent response time and also has a complex nonlinear correlation between current density and voltage. Dynamic electrochemical methods as such have more advantages over steady state measurements due to enabled frequency-response information [13]. Electrochemical impedance spectroscopy (EIS) is a commonly used, dynamic and frequency response method operating in a linear range, which is achieved by applying small excitation amplitude to a target system [14]. However, since the nonlinearity of the target system is neglected, EIS can hardly treat the full complexity of an electrochemical system. Therefore, extracting nonlinear response information has been recognized as an effective way to identify the electrochemical reaction mechanism [15–18].

Fig. 1 illustrates a schematic diagram of the voltage response of a PEMFC to a large-amplitude excitation current of sinusoidal form. The voltage response is displayed in both time domain and frequency domain. In the frequency domain, besides the response at the fundamental frequency, i.e. frequency of the excitation current, voltage contributions at the frequencies of higher harmonics are also observed. The harmonic frequencies are component frequencies that are the integer multiple of the fundamental frequency. The voltage intensity at the fundamental frequency is the linear part of the system response, which is used to calculate the linear frequency response of PEMFC, i.e. EIS. However, the responses at the higher harmonic frequencies are the nonlinear contribution of the system response, which can be used for evaluating nonlinearity and identifying reaction kinetics for complex electrochemical systems.

Vidaković-Koch et al. [17] applied second-order frequency response function (FRF) to evaluate the nonlinear behavior of a simple electrochemical system (i.e. ferrocyanide electrochemical oxidation) by means of FRF simulation. Panić et al. [18] further validated the simulation predictions by experimentally observed second-order FRF. It is suggested that plateaus and peaks observed in second-order FRF spectra are assignable to charge-transfer- or diffusion-induced nonlinearities. The second-order FRF spectra show more pronounced qualitative change originating from the reaction kinetics over the EIS. Wilson et al. [19] used both second-order and third-order harmonic spectra to describe the ORR process in solid oxide fuel cell. From the characteristics of the third-order harmonic spectra, the ORR on a perovskite oxide is suggested to be limited by oxygen dissociative adsorption. Bensmann et al. [20] also conducted a model-based analysis for methanol oxidation kinetics by means of the second-order FRF for a direct methanol fuel cell (DMFC) anode. The second order FRF was found different for each possible mechanism of the methanol oxidation process, which suggests that it can be used to discriminate the most likely reaction mechanisms for given kinetics. Kadyk et al. [16,21,22] extended the application of the second-order FRF to the state of art diagnosis for the PEMFC. According to their report, second-order FRF analysis proves to be a more effective way to make a distinction between CO-poisoned and dehydrated condition in comparison to the EIS.

Our previous research [15,23] also confirmed the advantage of the nonlinear frequency response on the kinetics discrimination by means of total harmonic distortion (THD) spectroscopy. THD is an effective method to evaluate nonlinearity of the target system that considers the contribution at all higher harmonic frequencies. It can be defined as the ratio of the Euclidean norm of the system response Y of all higher harmonic frequencies ($k \geq 2$) to that of the fundamental frequency ($k = 1$):

$$\mathrm{THD} = \frac{\sqrt{\sum_{k=2}^{\infty} Y_k^2}}{Y_1} \tag{6}$$

In our report, a three-step mechanism with Kauranen–Frumkin/Temkin kinetics was found to be more suitable to reproduce the methanol oxidation process. In addition, the monotonous correlation between the THD and the methanol inlet concentration at certain frequencies enable the THD analysis to sense methanol concentration during DMFC operation [23]. Ramschak patented the THD technique for monitoring the critical status of the PEMFC [24]. It is suggested that the deficiency of O_2 stoichiometry can be detected by THD spectra for the frequencies less than 30 Hz [25]. However, theoretical background for such detection has not been elucidated yet.

ORR is a kinetically slow process and as such dominates the overall performance of PEMFC. Damjanovic ORR mechanism with either oxygen electrochemisorption or oxygen chemisorption are two of the most likely mechanisms for the ORR at the PEMFC cathode. However, little work has been done on the difference in the dynamic response of the PEMFC with respective to mentioned ORR mechanisms. Therefore, many aspects of the electrochemical response of the PEMFC are still not fully understood, such as the cause of the THD variation of the PEMFC with O_2 stoichiometry [25] as well as the contribution of the cathodic ORR to the THD response of a DMFC [23]. Above pioneer researches have shown that higher order harmonic response information has obvious advantage on the identification of electrochemical reaction kinetics and system diagnosis over other commonly used electrochemical methods. Therefore, in order to contribute to the understanding, simulated THD spectra are used to demonstrate the difference in the dynamic response of a PEMFC with mentioned Damjanovic ORR mechanisms. ORR mechanism identification and the related discussion on the nonlinear frequency response behaviors of the PEMFC with O_2 stoichiometry will be proposed by comparing simulations with experimental THD spectra.

2. Simulation

2.1. Dynamic model of a PEMFC cathode with Damjanovic ORR mechanisms

Continuous stirred tank reactor (CSTR) network model, as shown in Fig. 2, is used for dynamic response behavior simulation for a PEMFC cathode. The cathode compartment is composed of cathode channel and cathode reaction zone (i.e. gas diffusion electrode). The cathode channel is assumed to be a network of CSTR modules in series, which could effectively reproduce the O_2 partial pressure variation along the single serpentine channel [23,26,27]. Each mentioned CSTR is also additionally connected to a CSTR that represents the associated cathode reaction zone. The volume of each CSTR in the cathode compartment is calculated as follows:

$$V^{i,\mathrm{CSTR}} = \frac{V^i}{n} \quad i = \mathrm{C\ or\ CR} \tag{7}$$

where the superscript C and CR represent the cathode channel and the cathode reaction zone, respectively. V is the volume and n is the number of CSTR modules of either cathode channel or cathode reaction zone. Similarly, the geometric electrode area of each CSTR segment is calculated by taking into account the whole area of the cathode (A_s) and the number of CSTRs, which is shown in Eq. (8):

$$A_s^{\mathrm{CSTR}} = \frac{A_s}{n} \tag{8}$$

In the simulation, cathode potential (E_c versus dynamic hydrogen reference electrode (DHE)) is identical for all CSTR segments. It

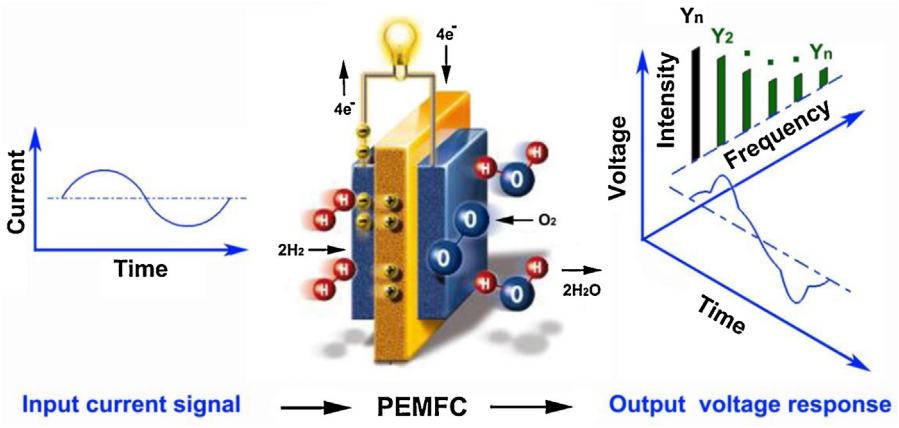

Fig. 1. Schematic diagram of the voltage response of a PEMFC in both time domain and frequency domain to a sinusoidal input of current.

correlates with the cathode overpotential, η_c, by means of Nernst equation:

$$\eta_c = E_c - E_c^{\varnothing} - \frac{RT}{zF} \ln\left(\frac{P_{O_2}^{CR}}{P^{\varnothing}}\right) \tag{9}$$

where $P_{O_2}^{CR}$ is the oxygen partial pressure in the cathode reaction zone. $E_c^{\varnothing}$ and $P^{\varnothing}$ are standard cathode potential of the ORR and the standard pressure, respectively. R, T and F are universal gas constant, absolute temperature and Faraday constant, respectively; z is the number of the electrons exchanged during the ORR process. The cathode current of all CSTR modules is summed to yield the total cell current:

$$A_s j_{cell} = \sum_{k}^{n} A_{cell}^{CSTR} j_{cell}^{k} \tag{10}$$

where j_{cell} and j_{cell}^{k} are the current density of the total electrode and that of CSTR segment k, respectively.

Damjanovic ORR mechanisms with either oxygen electrochemisorption or oxygen chemisorption are employed in the CSTR module for cathode reaction zone. Both of the oxygen adsorption processes are assumed under Temkin conditions, since most of the steady state voltage at the current density of 960 A m^{-2} for THD study is above 0.8 V, which is shown in Section 4.4. As for the electrochemical reduction of adsorbed O_2H, i.e. Eqs. (2) and (5), they are assumed to be three sequential one-electron-transfer reactions with the same reaction kinetics and under Langmuir conditions. Model equations of enrolled reaction steps are listed in Table 1. Table 2 lists the equations of the mass transfer process and charge transfer process in both cathode channel and cathode reaction zone, respectively. Maxwell–Stefan equation is used to model the diffusion of O_2, N_2 and H_2O vapor through the cathode reaction zone. With above dynamic model systems, the kinetics parameters of the ORR, as listed in Table 3, are obtained by fitting the model with steady state internal resistance (IR) corrected I–V curves at the O_2 stoichiometry of 6 by means of a global optimization method, which is composed of a random search using genetic algorithm and a local optimization employing a trust-region-reflective algorithm. In addition, parameter fitting is also performed for the oxygen electrochemisorption mechanism in which the adsorbed O_2H reduction step adopts the same parameters from the mechanism with oxygen chemisorption. Besides, a detailed variable and parameter declaration is given in the nomenclature.

2.2. THD spectra simulations for the PEMFC

THD simulations are achieved by applying a sinusoidal current to the dynamic equations of the PEMFC. The excitation current is:

$$j(t) = j_{dc} + j_{ac} \cdot \sin(\omega \cdot t) \tag{11}$$

The voltage response of the PEMFC cathode is then obtained in the time domain by solving the ordinary differential equations listed in Table 2. After expanding the time domain voltage response into a Fourier series, the voltage response of the cathode at the

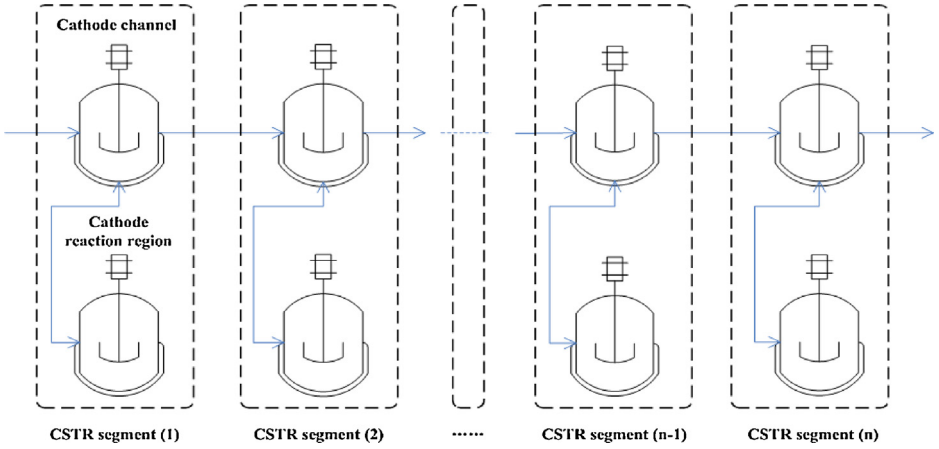

Fig. 2. CSTR network model for PEMFC cathode.

Table 1
ORR kinetic equations of the Damjanovic mechanism with different O_2 adsorption mode.

ORR mechanism with O_2 electrochemisorption	ORR mechanism with O_2 chemisorption
$R^i_{c1} = K_{101}\cdot(1-\theta^i_{O_2H})\cdot\left(\frac{P^{CR,i}_{O_2}}{P^{\Theta}}\right)\cdot\exp\left(-\beta_1\cdot r_1\cdot\frac{\theta^i_{O_2H}}{RT}\right)\cdot\exp\left(-\frac{(1-\beta_a)F}{RT}\eta_c\right)$ (T1.1)	$R^i_{c1} = K'_{101}\cdot(1-\theta^i_{O_2}-\theta^i_{O_2H})\cdot\left(\frac{P^{CR,i}_{O_2}}{P^{\Theta}}\right)\cdot\exp\left(-\beta_1\cdot r_1\cdot\frac{\theta^i_{O_2}}{RT}\right)$ (T1.5)
$R^i_{c2} = K_{102}\cdot\theta^i_{O_2H}\cdot\exp\left((1-\beta_1)\cdot r_1\cdot\frac{\theta^i_{O_2H}}{RT}\right)\cdot\exp\left(\frac{\beta_a F}{RT}\eta_c\right)$ (T1.2)	$R^i_{c2} = K'_{102}\cdot\theta^i_{O_2}\cdot\exp\left((1-\beta_1)\cdot r_1\cdot\frac{\theta^i_{O_2}}{RT}\right)$ (T1.6)
$R^i_{c3} = K_{201}\cdot\theta^i_{O_2H}\cdot\exp\left(-\frac{(1-\beta_a)F}{RT}\eta_c\right)$ (T1.3)	$R^i_{c3} = K'_{201}\cdot\theta^i_{O_2}\cdot\exp\left(-\frac{(1-\beta_a)F}{RT}\eta_c\right)$ (T1.7)
$R^i_{c4} = K_{202}\cdot(1-\theta^i_{O_2H})\cdot\exp\left(\frac{\beta_a F}{RT}\eta_c\right)$ (T1.4)	$R^i_{c4} = K'_{202}\cdot\theta^i_{O_2H}\cdot\exp\left(\frac{\beta_a F}{RT}\eta_c\right)$ (T1.8)
	$R^i_{c5} = K'_{301}\cdot\theta^i_{O_2H}\cdot\exp\left(-\frac{(1-\beta_a)F}{RT}\eta_c\right)$ (T1.9)
	$R^i_{c6} = K'_{302}\cdot(1-\theta^i_{O_2}-\theta^i_{O_2H})\cdot\exp\left(\frac{\beta_a F}{RT}\eta_c\right)$ (T1.10)

Table 2
Dynamic model equations for the PEMFC cathode.

Cathode channel	$\frac{dP^{C,i}_{O_2}}{dt} = \frac{F^{C,i}}{V^{C,CSTR}}(P^{C,in/(i-1)}_{O_2} - P^{C,i}_{O_2}) - \frac{J^i_{O_2}A^{CSTR}_S RT}{V^{C,CSTR}}$ (T2.1)	
	$\frac{dP^{C,i}_{N_2}}{dt} = \frac{F^{C,i}}{V^{C,CSTR}}(P^{C,in/(i-1)}_{N_2} - P^{C,i}_{N_2}) - \frac{J^i_{N_2}A^{CSTR}_S RT}{V^{C,CSTR}}$ (T2.2)	
	$\frac{dP^{C,i}}{dt} = \frac{F^{C,i}}{V^{C,CSTR}}(P^{C,in/(i-1)} - P^{C,i}) - \frac{R^i_{c1}A^{CSTR}_S RT}{V^{C,CSTR}}$ (T2.3)	
	ORR mechanism with O_2 electrochemisorption	**ORR mechanism with O_2 chemisorption**
Cathode reaction zone	$C_{PtO_2H}\frac{d\theta^{CR,i}_{O_2H}}{dt} = R^i_{c1} - R^i_{c2} - R^i_{c3} + R^i_{c4}$ (T2.4)	$C_{PtO_2}\frac{d\theta^{CR,i}_{O_2}}{dt} = R^i_{c1} - R^i_{c2} - R^i_{c3} + R^i_{c4}$ (T2.6)
	$C_{dl}\frac{d\eta_c}{dt} = j(t) - \sum_{i=1}^{n}((R^i_{c1} - R^i_{c2}) + 3(R^i_{c3} - R^i_{c4}))\cdot\frac{F}{n}$ (T2.5)	$C_{PtO_2H}\frac{d\theta^{CR,i}_{O_2H}}{dt} = R^i_{c3} - R^i_{c4} - R^i_{c5} + R^i_{c6}$ (T2.7)
		$C_{dl}\frac{d\eta_c}{dt} = j(t) - \sum_{i=1}^{n}((R^i_{c3} - R^i_{c4}) + 3(R^i_{c5} - R^i_{c6}))\cdot\frac{F}{n}$ (T2.8)
	$\frac{dP^{CR,i}_{O_2}}{dt} = \frac{J^i_{O_2}A^{CSTR}_S RT}{V^{C,CSTR}} - \frac{R^i_{c1}A^{CSTR}_S RT}{V^{C,CSTR}}$ (T2.9)	
	$\frac{dP^{CR,i}_{N_2}}{dt} = \frac{J^i_{N_2}A^{CSTR}_S RT}{V^{C,CSTR}}$ (T2.10)	
	$0 = \frac{A_s(P^{CR,i}_{O_2} - P^{C,i}_{O_2})}{RTV^{CR,CSTR}} + \frac{x^i_{H_2O}\cdot J^i_{O_2} - x^i_{O_2}\cdot J^i_{H_2O}}{D_{O_2,H_2O}} + \frac{x^i_{N_2}\cdot J^i_{O_2} - x^i_{O_2}\cdot J^i_{N_2}}{D_{O_2,N_2}}$ (T2.11)	
	$0 = \frac{A_s(P^{CR,i}_{N_2} - P^{C,i}_{N_2})}{RTV^{CR,CSTR}} + \frac{x^i_{H_2O}\cdot J^i_{N_2} - x^i_{N_2}\cdot J^i_{H_2O}}{D_{N_2,H_2O}} + \frac{x^i_{O_2}\cdot J^i_{N_2} - x^i_{N_2}\cdot J^i_{O_2}}{D_{N_2,O_2}}$ (T2.12)	
	$0 = J^i_{O_2} + J^i_{N_2} + J^i_{H_2O} - R^i_{c1}$ (T2.13)	
	$1 = x^i_{O_2} + x^i_{N_2} + x^i_{H_2O}$ (T2.14)	

Table 3
ORR kinetics parameters obtained by global optimization methods.

O_2 electrochemisorption [mol s^{-1} m^{-2}]			O_2 chemisorption [mol s^{-1} m^{-2}]	
K_{101}	9.113×10^{-5}	1.590×10^{-5}	K'_{101}	3.560×10^{3}
K_{102}	1.342×10^{-20}	5.060×10^{-22}	K'_{102}	1.197×10^{-6}
K_{201}	9.614×10^{-5}	2.033×10^{-3}	K'_{201}	1.655×10^{-5}
K_{202}	1.282×10^{-1}	6.977×10^{-16}	K'_{202}	6.381×10^{1}
		Assuming: $K_{201} = K'_{301}$	K'_{301}	2.033×10^{-3}
		$K_{202} = K'_{302}$	K'_{302}	6.977×10^{-16}

fundamental frequency and that at higher harmonic frequencies are obtained as:

$$E_c = E_{c,dc} + \sum_{k=1}^{\infty}(E_{cc,k}\varphi_k(t) + E_{cs,k}\psi_k(t)) \quad (12)$$

where φ_k and ψ_k are normalized basis functions, which are given by Eqs. (13) and (14), respectively. The subscript k is the order of the Fourier approximation, which ranges over the integers.

$$\varphi_k(t) = \sqrt{\frac{\omega}{\pi}}\cos(k\omega t) \quad (13)$$

$$_k(t) = \sqrt{\frac{\omega}{\pi}}\sin(k\omega t) \quad (14)$$

$E_{c,dc}$ is the steady state value of cathode potential. The coefficients $E_{cc,k}$ (of the cos-terms) and $E_{cs,k}$ (of the sin-terms) are given by the following integrals:

$$E_{cc,k} = \int_0^T E_c(t)\cdot\varphi_k(t)dt \quad (15)$$

$$E_{cs,k} = \int_0^T E_c(t)\cdot\psi_k(t)dt \quad (16)$$

Therefore, the Fourier series can be rewritten as:

$$E_c(t) = E_{c,dc} + \sum_{k=1}^{\infty} E_{total,ck}\sqrt{\frac{\omega}{\pi}}\sin(k\omega t + \vartheta_k) \quad (17)$$

with

$$E_{total,ck} = \sqrt{E_{cc,k}^2 + E_{cs,k}^2} \quad (18)$$

where $E_{total,ck}$ is the root of summed squares of the cathode voltage amplitude at angular frequency $k\omega$; ϑ_k is the phase shift.

H_2 oxidation reaction in PEMFC anode is a fast process due to the high exchange current density on platinum surface [28]. Under the condition of high H_2 stoichiometry, the anode can be taken as a dynamic hydrogen reference electrode (DHE) and has negligible contribution to the THD signals. This fact will be discussed in Section 4.3 in detail. Based on the definition of THD, i.e. Eq. (6), $E_{total,ck}$ corresponds to Y_k when $k \geq 2$. However, as for the response at the fundamental frequency, the ohmic loss of the electrolyte membrane should be considered. Therefore, E_1, corresponding to Y_1, is shown in the following:

$$E_1(t) = E_{c,k=1} + R_{mem}\cdot(j_{dc} + j_{ac}\sin(\omega t)) \quad (19)$$

In addition, the apparent double layer capacitance is optimized by matching frequency at the minimum phase angle of the EIS between simulation and experiment at O_2 stoichiometry of 6. As such, the magnitude of the electrochemical impedance of the PEMFC can be calculated by using the voltage response at the fundamental frequency and the input current:

$$|Z| = \frac{\sqrt{\left(E_{cc,1}\cdot\sqrt{\omega/\pi}\right)^2 + \left(E_{cs,1}\cdot\sqrt{\omega/\pi} + j_{ac}R_{mem}\right)^2}}{j_{ac}} \quad (20)$$

THD of the PEMFC is:

$$\mathrm{THD} = \frac{\sqrt{\sum_{k=2}^{\infty} E_{total,ck}^2}}{\sqrt{\left(E_{cc,1}\cdot\sqrt{\omega/\pi}\right)^2 + \left(E_{cs,1}\cdot\sqrt{\omega/\pi} + j_{ac}R_{mem}\right)^2}} \quad (21)$$

In this article, the simulated voltage amplitudes ranging from the fundamental frequency to the 10th harmonic frequency are used to calculate the THD. All simulations were performed using a commercial software package (MATLAB R2010b, the MathWorks Inc.). The relative error tolerance for the initial value problem of ordinary differential equations is 10^{-12}.

3. Experimental

A commercial membrane electrode assembly (MEA, type M241) from Johnson Matthey Co. was used for all measurements. PtRu/C and Pt/C are employed as the catalysts for the anode and the cathode, respectively. Nafion®-115 membrane is used as the electrolyte. The apparent MEA area is 26 cm^2. The single cell was completed by sandwiching the MEA between the two carbon plates with a single serpentine channel each, gold-plated copper current collectors and stainless steel end plates.

The cathode of the PEMFC single cell was supplied by humidified gas mixture of N_2 and O_2 at 60 °C with a total flow rate of 276.5 standard cubic centimeters per minute (SCCM). O_2 stoichiometry was adjusted by changing the flow rate ratio of O_2 to N_2. The anode was fed by humidified H_2 at 60 °C with a flow rate of 500 SCCM. The PEMFC was operated in the fuel cell mode at 60 °C. Steady state *I–V* curves of the MEA were measured by a potentiostat from Zahner-Elektrik (Zennium and PP241). EIS and THD spectra were measured by the Zahner impedance measurement unit. Amplitude of 38 A m^{-2} and frequency range from 1×10^4 Hz to 1×10^2 Hz were used for the EIS measurement to obtain internal resistance of the PEMFC at different offset current densities for IR corrected *I–V* curve calculations. However, amplitude of 380 A m^{-2} and frequency range from 5×10^4 Hz to 1×10^{-2} Hz were employed for THD and comparable EIS studies. As for the latter, the voltage responses of the PEMFC from the 1st harmonic to the 10th harmonic were recorded to obtain the THD spectrum. The offset current density is selected at 960 A m^{-2}. The relatively low current density is not only helpful to obtain more pronounced THD response [29], but can avoid serious cell potential fluctuation caused by cathode flooding at relatively high current densities [30]. Additionally, THD measurements were also performed for H_2/H_2 cell in electrolysis cell mode, in which humidified H_2 at 60 °C with a flow rate of 500 SCCM was fed to both cathode and anode. To check the data accuracy of the steady state *I–V* curves, EIS and the THD spectra, each measurement was repeated three times. The error is represented by the error bar in the diagram.

4. Results and discussion

4.1. Simulations of steady state I–V curve and EIS for the PEMFC with Damjanovic ORR mechanisms

Steady state *I–V* relation and EIS are commonly used in the kinetic research of electrochemical reactions. With the cathode model introduced in Section 2, steady state IR corrected *I–V* curve and EIS of the PEMFC are simulated for both options of Damjanovic ORR mechanism and different O_2 stoichiometry, respectively. Fig. 3(a) and (b) shows simulated IR corrected *I–V* curves of the PEMFC that employ the ORR mechanisms with oxygen electrochemisorption and with oxygen chemisorption, respectively. The experimental results of the PEMFC at O_2 stoichiometries of 6 and 1.5 are also shown in both figures. It can be observed that the IR corrected cell potential apparently decreases with decrease in O_2 stoichiometry for both options of ORR mechanism; the simulated I–V curves fit with the experimental results well at the O_2 stoichiometry of 6. When the O_2 stoichiometry is 1.5, the simulation adopting the ORR mechanism with oxygen chemisorption agrees with the experiments better than that with oxygen electrochemisorption. However, it could not be used to identify the ORR kinetics qualitatively.

Fig. 4 shows simulated linear frequency response of the PEMFC, i.e. magnitude ($|Z|$) of the EIS, at the offset current density of 960 A m^{-2}. Subfigures (a) and (b) show the simulation results when the simulation adopts the ORR mechanism with oxygen electrochemisorption and oxygen chemisorption, respectively. It can be observed that $|Z|$ shows similar tendency with O_2 stoichiometry for both options of ORR mechanism. It increases with decreased O_2 stoichiometry in the low frequency region (from 0.01 Hz to 0.86 Hz for the mechanism with oxygen electrochemisorption; from 0.01 Hz to 0.63 Hz for the mechanism with oxygen chemisorption). However, in the middle frequency region (from 1.6 Hz to 5 Hz), $|Z|$ decreases with decreased O_2 stoichiometry for both options

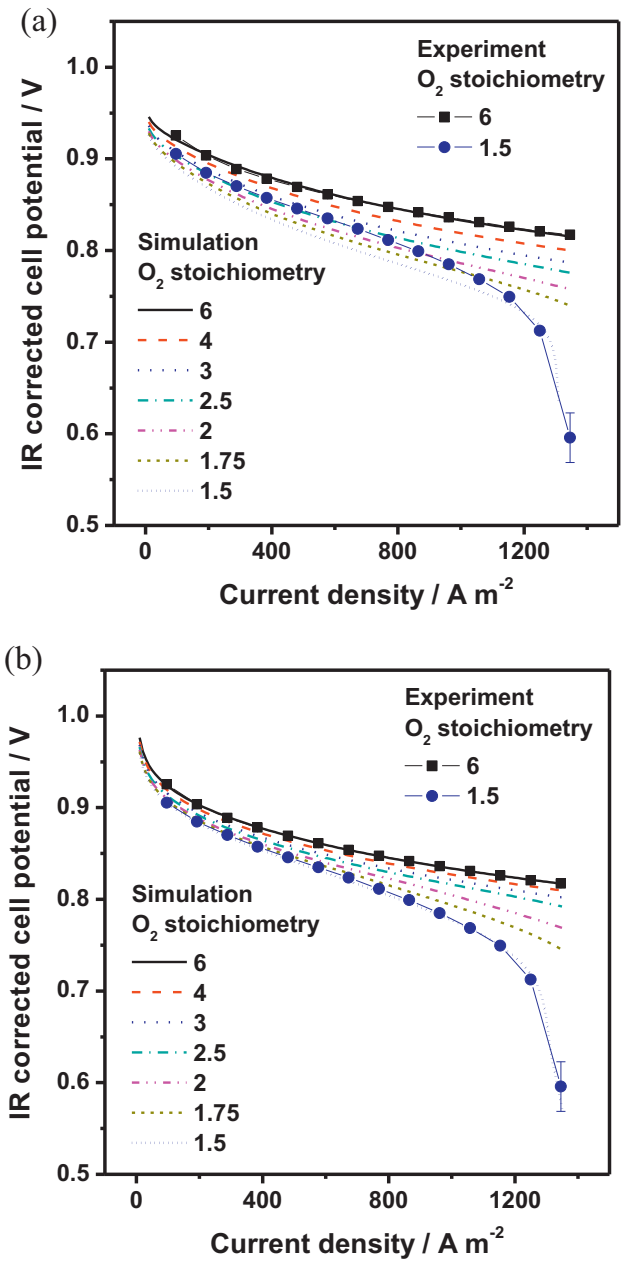

Fig. 3. Simulated IR corrected steady-state *I–V* curves of the PEMFC with different O_2 stoichiometry at 60 °C as well as the experimental results at the O_2 stoichiometries of 6 and 1.5: (a) Damjanovic ORR mechanism with oxygen electrochemisorption and (b) Damjanovic ORR mechanism with oxygen chemisorption.

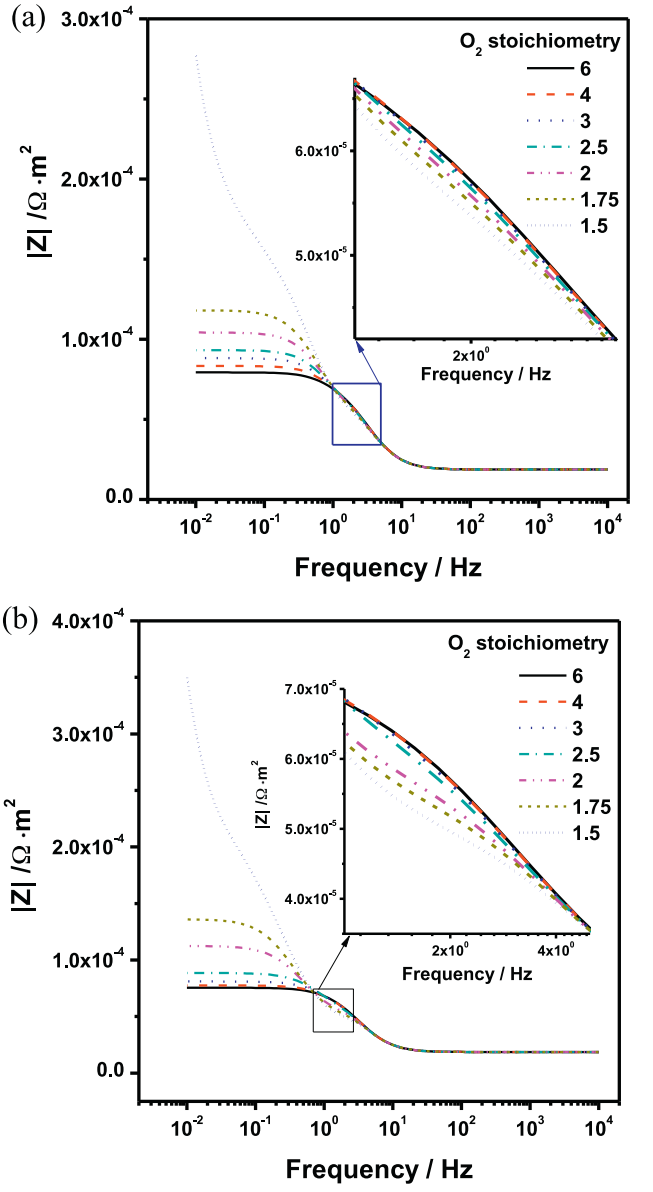

Fig. 4. Simulated linear frequency response of the PEMFC, i.e. |*Z*| versus frequency, with different O_2 stoichiometry at 60 °C: (a) Damjanovic ORR mechanism with oxygen electrochemisorption and (b) Damjanovic ORR mechanism with oxygen chemisorption.

of ORR mechanism. In the high frequency region (higher than 5 Hz), the difference of the |*Z*| with O_2 stoichiometry could not be distinguished obviously.

From the simulations above, it is concluded that the steady state *I–V* curve and the linear frequency response of the PEMFC cannot be used to distinguish the ORR mechanisms with different oxygen adsorption processes qualitatively, when the O_2 stoichiometry is taken as the adjustable parameter. Lack of the time scale information and the linear target assumption are further confirmed to be the proposed reasons for the steady state *I–V* curve and the EIS failing to deal with distinguishing the complex electrochemical reaction mechanisms, respectively. Therefore, extracting nonlinear response information became necessary to treat with the complex kinetics of electrochemical systems.

4.2. Simulations of THD spectroscopy and kinetic parameters analysis for the PEMFC with Damjanovic ORR mechanisms

THD spectroscopy contains nonlinear frequency response information of a target system [15,23]. Fig. 5(a) and (b) shows simulated THD spectra of a PEMFC which adopts the ORR mechanisms mentioned above in the frequency range from 0.01 Hz to 25 Hz, respectively. The frequency range is nonlinear response term sensitive, which will be discussed in Section 4.3. It can be observed that the THD shows different variation with O_2 stoichiometry for different ORR mechanisms.

As for the mechanism with oxygen electrochemisorption, which is shown in Fig. 5(a), THD decreases in the frequency range from 0.01 Hz to 10 Hz when O_2 stoichiometry decreases from 6 to 2. In the frequency range from 0.74 Hz to 10 Hz, THD values continue to decrease with further decrease in O_2 stoichiometry. However, a pronounced increase can be observed for the frequencies less than

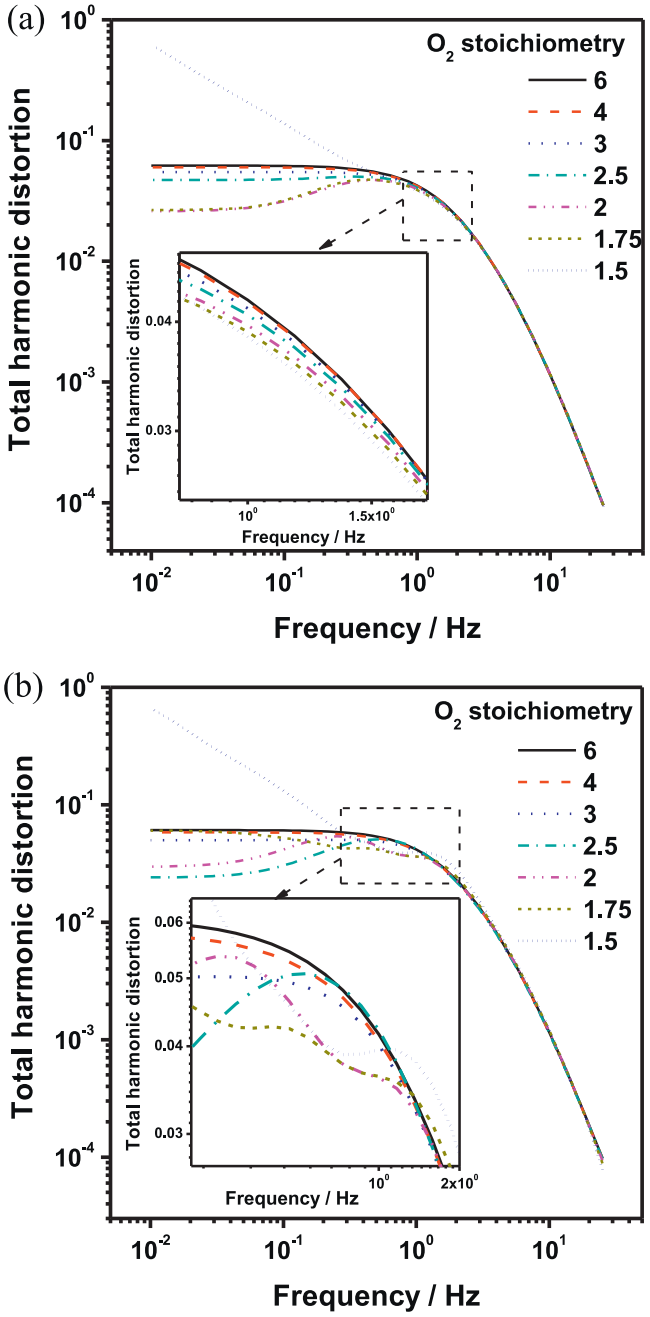

Fig. 5. Simulated THD spectra of the PEMFC with different O_2 stoichiometry at 60 °C: (a) Damjanovic ORR mechanism with oxygen electrochemisorption and (b) Damjanovic ORR mechanism with oxygen chemisorption.

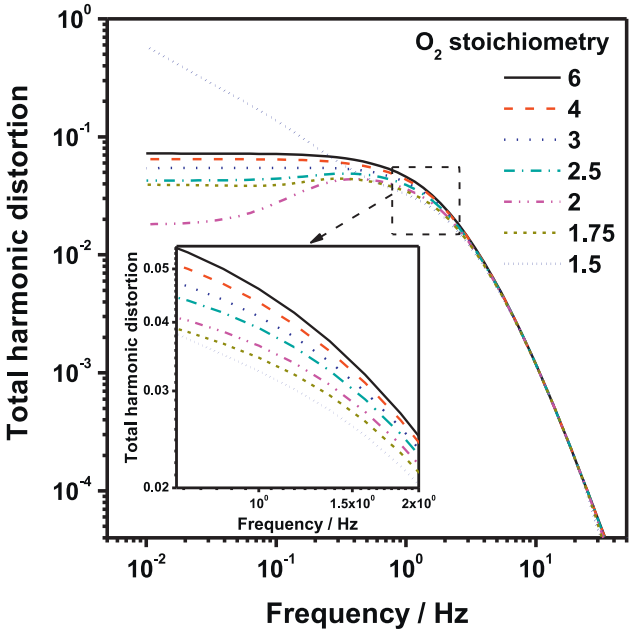

Fig. 6. Simulated THD spectra of the PEMFC for the ORR mechanism with oxygen electrochemisorption in which the adsorbed O_2H reduction step adopts the kinetic parameters from the mechanism with oxygen chemisorption.

0.74 Hz at the O_2 stoichiometry of 1.5. A THD peak around 0.5 Hz appears for O_2 stoichiometries below 3.

Fig. 5(b) shows the THD spectra for the ORR mechanism with oxygen chemisorption. In the frequency range less than 10 Hz, THD decreases when O_2 stoichiometry decreases from 6 to 3. A plateau and a low frequency asymptote can be observed in this frequency range. With further decrease in O_2 stoichiometry, the THD spectra demonstrate more complex variation. For the frequencies less than 0.16 Hz, THD decreases when O_2 stoichiometry decreases from 6 to 2.5 and then increases with further decrease in O_2 stoichiometry. However, in the higher frequency range, THD peaks around 0.54 Hz, 0.25 Hz and 1.16 Hz are observed for the O_2 stoichiometries of 2.5, 2 and 1.5, respectively. Two THD peaks at 0.46 Hz and 1.0 Hz can be distinguished in the THD spectrum at the O_2 stoichiometry of 1.75. Compared with the THD spectrum at the O_2 stoichiometry of 6, an obvious higher THD value can be observed in the frequency range from 1.35 Hz to 10 Hz and from 1.16 Hz to 10 Hz for the O_2 stoichiometries of 1.75 and 1.5, respectively.

ORR kinetic parameters for both options of ORR mechanism are listed in Table 3; they were obtained by fitting the experimental IR corrected *I–V* curve of the PEMFC at the O_2 stoichiometry of 6 and using global optimization. It can be observed that, besides the difference in the oxygen adsorption steps, kinetic parameters of the adsorbed O_2H reduction step (Eqs. (2) and (5)) are also different in several orders of magnitude from each other. Therefore, the O_2H reduction step might also influence the dynamic response behavior of the ORR process. In order to identify the cause for the difference between the simulated THD spectra shown in Fig. 5(a) and (b), an additional simulation for the ORR mechanism with oxygen electrochemisorption is performed using partly identical and partly optimized kinetic parameters. In the simulation, the adsorbed O_2H reduction step adopts the kinetic parameters obtained from the mechanism with oxygen chemisorptions, which are also listed in Table 3. Fig. 6 shows the simulated THD spectra. It is obvious that THD decreases first and then increase for frequencies less than 0.54 Hz as well as decreases monotonously in the frequency range from 0.63 Hz to 10 Hz with decreased O_2 stoichiometry. Therefore, Fig. 6 demonstrates the same tendency with the THD spectra shown in Fig. 5(a), which not only indicates that the different features observed between the THD spectra shown in Fig. 5(a) and (b) are of qualitative nature of ORR mechanism, but also clarifies that the complex THD response observed in the frequency range from 1.16 Hz to 10 Hz in the simulation for the mechanism with oxygen chemisorption originates from oxygen adsorption steps rather than from the adsorbed O_2H reduction step. Therefore, it can be concluded that THD spectroscopy has the ability to demonstrate the difference of the Damjanovic ORR mechanism with different oxygen adsorption processes in certain frequency ranges.

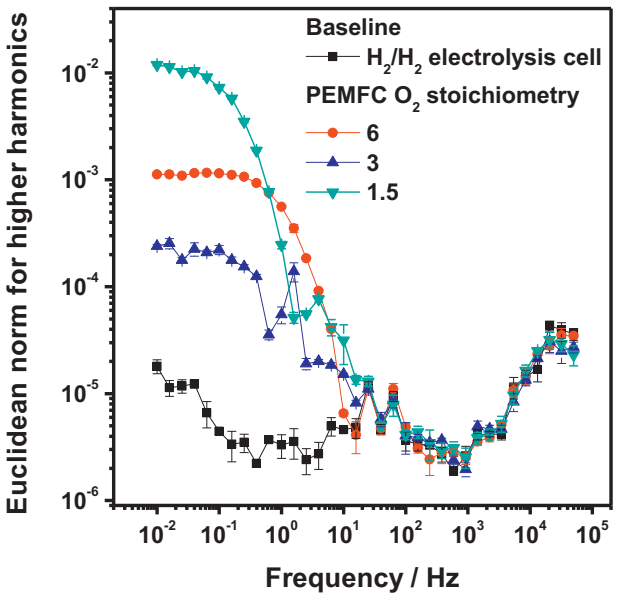

Fig. 7. Experimental Euclidean norm $\left(\sqrt{\sum_{k=2}^{10} E_{\text{total},ck}^2}\right)$ spectra for the higher harmonic voltage response of the H_2/H_2 electrolysis cell and that of the PEMFC with different O_2 stoichiometry.

4.3. Experimental separation of ORR contribution from system error in THD spectroscopy

The numerator of the defined THD for the PEMFC in Eq. (21), $\sqrt{\sum_{k=2}^{\infty} E_{\text{total},ck}^2}$, contains the contribution of the nonlinear terms to the dynamic behavior of the PEMFC. According to our previous reports [23], the Euclidean norm is sensitive to the current amplitude and can be distinguished from the system noise by comparing to the H_2/H_2 electrolysis cell. Fig. 7 shows the experimental Euclidean norm spectra of the H_2/H_2 electrolysis cell and that of the PEMFC with three different O_2 stoichiometries. It can be observed that the difference of the norm values between the H_2/H_2 electrolysis cell and the PEMFC could not be distinguished for frequencies higher than 15.8 Hz. The magnitude of the Euclidean norm of the H_2/H_2 electrolysis cell and the PEMFC is in the range of 2×10^{-6}–4×10^{-5}. For the frequencies less than 15.8 Hz, the Euclidean norms of the H_2/H_2 electrolysis cell also keep in the same range of the magnitude. However, that of the PEMFC increases strongly with decrease in frequency. A low frequency asymptote and a plateau with a magnitude about 1×10^{-3} can be observed in the Euclidean norm spectra of the PEMFC at the O_2 stoichiometry of 6. When O_2 stoichiometry decreases to 3 and 1.5, besides the low frequency asymptote, an additional peak can be also observed around 1.6 Hz and 4.0 Hz, respectively.

Proton transfer in Nafion® membrane obeys Ohm's law, which is a linear process and should not contribute to the Euclidean norm spectra [23]. H_2 redox reaction on Pt surface is a fast process due to the high exchange current density. Although two-step mechanisms (i.e. Volmer–Tafel and Volmer–Heyrovsky) are found more suitable for the H_2 evolution process [31,32], the experimental norm spectra of the H_2/H_2 electrolysis cell indicates it also contributes negligibly to the PEMFC nonlinear response when the H_2 stoichiometry is high. Therefore, the Euclidean norm spectrum of the H_2/H_2 electrolysis cell is comparable to the system error arising from the anode, membrane, fuel cell assembly or the resolution of the measuring instruments themselves. Compared with the noise baseline presented by the H_2/H_2 electrolysis cell, it can be concluded that the Euclidean norm spectra of the PEMFC can be detected for frequencies less than 15.8 Hz when the current amplitude is 380 A m^{-2}.

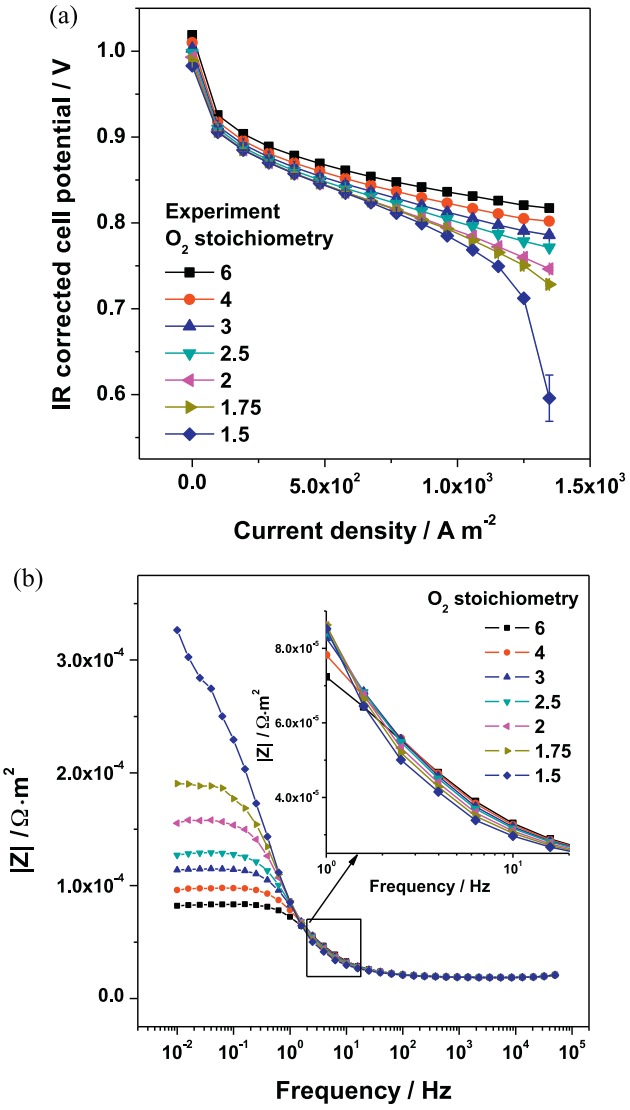

Fig. 8. Experimental IR corrected steady-state *I–V* curve and linear frequency response of the PEMFC, i.e. $|Z|$ versus frequency, with different O_2 stoichiometry: (a) IR corrected steady-state *I–V* curve and (b) linear frequency response.

4.4. Experimental validation of steady state and dynamic response for the PEMFC

Fig. 8(a) shows IR corrected *I–V* curves of the PEMFC with different O_2 stoichiometry. IR corrected cell potential apparently decreases with decrease in the O_2 stoichiometry, which demonstrates the same tendency with the simulations using both options of ORR mechanism as shown in Fig. 3(a) and (b), respectively. Fig. 8(b) shows the linear frequency response of the PEMFC, i.e. $|Z|$ of the EIS versus frequency. $|Z|$ increases with decreased O_2 stoichiometry in the frequency range from 0.01 Hz to 0.63 Hz and decreases in the frequency range from 4 Hz to 40 Hz. Compared with the simulated results shown in Fig. 4(a) and (b), the experimental results are also well reproduced by the simulation employing both options of ORR mechanism, qualitatively.

Fig. 9 shows the experimental THD spectra in the frequency range from 0.01 Hz to 40 Hz. The variation of the THD spectra with O_2 stoichiometry can be observed obviously for the frequencies less than 15.8 Hz, which presents the identical frequency range with

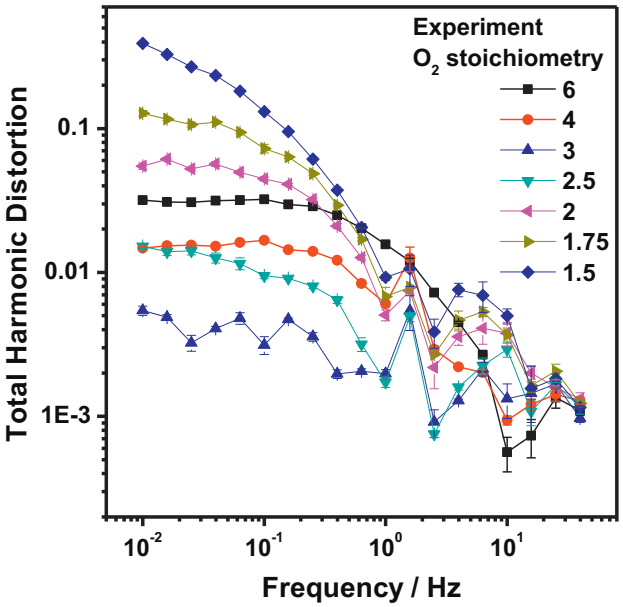

Fig. 9. Experimental THD spectra of the PEMFC with different O_2 stoichiometry at 60 °C.

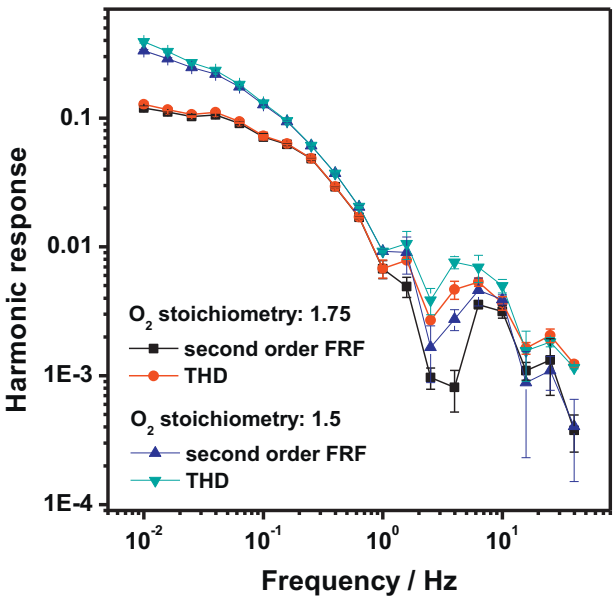

Fig. 10. Experimental E_2/E_1 spectra and THD spectra of the PEMFC at O_2 stoichiometry of 1.75 and 1.5 and at 60 °C.

the distinguishable Euclidean norm spectra of PEMFC as shown in Fig. 7. In the frequency range from 0.01 Hz to 0.63 Hz, THD decreases when O_2 stoichiometry decreases from 6 to 3 and then increases with further decrease in O_2 stoichiometry. Plateaus and low frequency asymptotes can be observed in this frequency range. At the frequency of 1.6 Hz, a sharp peak can be seen when the stoichiometry is less than 4. Moreover, in the frequency range from 2.5 Hz to 15.8 Hz, a broader peak is observed in the THD spectra when the O_2 stoichiometry is below 2.5. The THD peak increases with decrease in O_2 stoichiometry. Since the peak value appears at different frequencies, THD also shows non-monotonous relationship with O_2 stoichiometry in this frequency range.

It is obvious that the experimental THD spectra can be reproduced qualitatively by the simulation employing the Damjanovic ORR mechanism with oxygen chemisorption: the THD tendency for frequencies less than 0.63 Hz (i.e. decrease first and then increase) with decreased O_2 stoichiometry and the THD peak in the frequency range from 2.5 Hz to 15.8 Hz obviously observed at low O_2 stoichiometries (i.e. 1.75 and 1.5) are qualitatively reproduced by the simulations regarding this mechanism in the frequency less than 0.16 Hz and in the frequency range from 1.16 Hz to 10 Hz, respectively. Panić et al. [18] also recognized similar peaks in the experimental second order FRF spectra of the ferrocyanide electrochemical oxidation process when the mass transfer condition is changed. It is suggested that the peaks intensity of the second order FRF amplitude spectra from 1 Hz to 10 Hz is influenced by both charge transport parameter (i.e. reaction kinetics) and mass transport parameter. Fig. 10 shows the difference of the THD spectra of the PEMFC and the contribution part from second order FRF, i.e. E_2/E_1 spectra, at O_2 stoichiometry of 1.75 and 1.5. It can be observed that the second order FRF contributes mostly to the nonlinear response part of the THD. In logarithmic coordinate, the difference between the E_2/E_1 and the THD can be neglected in the frequency range from 0.01 Hz to 1 Hz, however, it can be observed clearly in the frequency range from 1 Hz to 15.8 Hz. Compared with THD spectra, E_2/E_1 spectra of the PEMFC show the same tendency, but less pronounced difference when the O_2 stoichiometry is changed. Therefore, it is reasonable to believe the peaks of the THD observed in the frequency from 2.5 Hz to 15.8 Hz are the fingerprint of the nonlinear response of the ORR process. Damjanovic ORR mechanism with oxygen chemisorptions is therefore suggested being as the better option to illustrate the ORR process at the PEMFC cathode, since observed experimental steady state, linear frequency response and nonlinear frequency response of the PEMFC are all qualitatively reproduced by the simulation regarding this mechanism.

With above THD simulations and experimental validations, nonlinear response behavior of the PEMFC can be well predicted and understood. The question in the section of introduction with regards to O_2 stoichiometry detection using THD spectra can be therefore solved. Previous research inferred that THD analysis can be used to monitor the critical status of PEMFC owing to insufficient O_2 stoichiometry [24]. This fact can be confirmed by both simulations and experimental THD spectra at the O_2 stoichiometry of 1.5. However, THD spectra show a more complex variation with decreased O_2 stoichiometry rather than a simple monotonous increase. The observed non-monotonous relationship between THD spectra and O_2 stoichiometry in both simulation (Fig. 5(b)) and experiment (Fig. 9) indicates that THD spectroscopy analysis is not suitable as a diagnosis method to quantify the O_2 concentration in the PEMFC under the offset current density of 960 A m^{-2}, when O_2 stoichiometry varies over a range from 4 to 2.5.

5. Conclusions

In this study, Damjanovic ORR mechanisms with oxygen electrochemisorption and oxygen chemisorption are comparatively studied by means of total harmonic distortion spectroscopy and commonly used steady state *I–V* curves and EIS. Numerical simulations and experimental validations are both employed to demonstrate the difference between the ORR mechanisms and to indentify the closer one to the reality, respectively. From simulations, only the THD spectroscopy that contains the nonlinear response information of electrochemical reactions enables a fine distinction for the most likely ORR mechanisms. With the help of experimental validation, the frequency range from 2.5 Hz to 15.8 Hz is recognized to be ORR kinetics sensitive in the THD spectroscopy. The Damjanovic ORR mechanism with oxygen chemisorption is comparable to the reality because it better reproduces experimental steady state, linear and nonlinear frequency response behavior of the PEMFC.

Acknowledgements

The authors acknowledge the support of this work by the Alexander von Humboldt Foundation and thank Dr. Vladimir Panić for the fruitful discussion in the field of nonlinear frequency response analysis.

Appendix A. Nomenclature

A_s	geometric electrode area of the PEMFC, 2.6×10^{-3} (m^2)
A_s^{CSTR}	geometric electrode area of a CSTR segment (m^2)
C_{dl}	apparent double layer capacitance, 8567 ($F\,m^{-2}$)
C_{PtO_2}	O_2 surface concentration on Pt surface, 0.00117 ($mol\,m^{-2}$)
C_{PtO_2H}	O_2H surface concentration on Pt surface, 0.002 ($mol\,m^{-2}$)
d_{CR}	thickness of cathode reaction zone, 230×10^{-6} (m)
$D_{x,y}$	binary gas diffusivity coefficient for species x and y ($m^2\,s^{-1}$) [33]
E_c	cathode potential (V)
F	Faraday constant, 96,485 ($C\,mol^{-1}$)
j_{cell}	cell current density, 960 ($A\,m^{-2}$)
j_{cell}^i	cell current density of the CSTR segment i ($A\,m^{-2}$)
J_y^i	flux of species y in cathode reaction zone of CSTR module i ($mol\,m^{-2}\,s^{-1}$)
K_n	reaction rate constant for cathode reaction step n for the ORR mechanism with active oxygen adsorption
K_n'	reaction rate constant for cathode reaction step n for the ORR mechanism with non-active oxygen adsorption.
n	numbers of CSTR segment, 7
$P^{\varnothing}$	standard pressure, 101,325 (Pa)
$P_y^{C,i}$	pressure of species y in cathode channel of CSTR module i (Pa)
$P_y^{CR,i}$	pressure of species y in cathode reaction zone of CSTR module i (Pa)
r_1	rate of the change of the free energy of adsorption with coverage 2.52×10^5 ($J\,mol^{-1}$)
R_{cn}^i	electrochemical reaction rate of cathode reaction step n in CSTR module i ($mol\,m^{-2}\,s^{-1}$)
R	universal gas constant, 8.314 ($J\,mol^{-1}\,K^{-1}$)
R_{mem}	membrane resistance, 1.867×10^{-6} ($\Omega\,m^2$)
t	time (s)
T	cell temperature, 333.15 (K)
V^C	volume of cathode channel, 1.385×10^{-6} (m^3)
$V^{C,CSTR}$	volume of cathode channel region in a CSTR module (m^3)
V^{CR}	volume of cathode reaction zone, 6.24×10^{-7} (m^3)
$V^{CR,CSTR}$	volume of cathode reaction zone in a CSTR module (m^3)
x_y^i	molar fraction of species y in cathode reaction zone of CSTR module i
$\|Z\|$	magnitude of the electrochemical impedance ($\Omega\,m^2$)
η_C^i	cathode overpotential of CSTR module i (V)
β_a	symmetry factor of ORR reaction in anodic direction, 0.5
β_1	symmetry factor for Temkin adsorption on Pt, 0.5
ε	porosity of anode reaction region, 0.75
$\theta_{O_2}^i$	surface coverage of adsorpted O_2 in CSTR module i
$\theta_{O_2H}^i$	surface coverage of adsorpted O_2H in CSTR module i

Superscripts

C	cathode channel
CR	cathode reaction zone
C, in	entering the cathode compartment
CSTR	CSTR module

References

[1] P. Fischer, J. Heitbaum, Mechanistic aspects of cathodic oxygen reduction, Electroanalytical Chemistry 112 (1980) 231.
[2] N.M. Markovic, T.J. Schmidt, V. Stamenkovic, P.N. Ross, Oxygen reduction reaction on Pt and Pt bimetallic surfaces: a selective review, Fuel Cells 1 (2001) 105.
[3] C.O. Laoire, S. Mukerjee, K.M. Abraham, Elucidating the mechanism of oxygen reduction for lithium–air battery applications, Journal of Physical Chemistry C 113 (2009) 20127.
[4] Q. Mao, G.Q. Sun, S.L. Wang, H. Sun, G.X. Wang, Y. Gao, A.W. Ye, Y. Tian, Q. Xin, Comparative studies of configurations and preparation methods for direct methanol fuel cell electrodes, Electrochimica Acta 52 (2007) 6763.
[5] Q. Mao, G.Q. Sun, S.L. Wang, H. Sun, Y. Tian, J. Tian, Q. Xin, Application of hyperdispersant to the cathode diffusion layer for direct methanol fuel cell, Journal of Power Sources 175 (2008) 826.
[6] S. Mukerjee, S. Srinivasan, Enhanced electrocatalysis of oxygen reduction on platinum alloys in proton-exchange membrane fuel cells, Journal of Electroanalytical Chemistry 357 (1993) 201.
[7] V.R. Stamenkovic, B. Fowler, B.S. Mun, G. Wang, P.N. Ross, C.A. Lucas, N.M. Marković, Improved oxygen reduction activity on $Pt_3Ni(1\,1\,1)$ via increased surface site availability, Science 315 (2007) 493.
[8] H.A. Gasteiger, S.S. Kocha, B. Sompalli, F.T. Wagner, Activity benchmarks and requirements for Pt, Pt-alloy, and non-Pt oxygen reduction catalysts for PEMFCs, Applied Catalysis B: Environmental 56 (2005) 9.
[9] A. Damjanovic, A. Dey, J. Bockris, Kinetics of oxygen evolution and dissolution on platinum electrodes, Electrochimica Acta 11 (1966) 791.
[10] O. Antoine, Y. Bultel, R. Durand, Oxygen reduction reaction kinetics and mechanism on platinum nanoparticles inside Nafion®, Journal of Electroanalytical Chemistry 499 (2001) 85.
[11] A. Damjanovic, V. Brusic, Electrode kinetics of oxygen reduction on oxide-free platinum electrodes, Electrochimica Acta 12 (1966) 615.
[12] M. Paucirova, D.M. Drazic, A. Damjanovic, The effect of surface coverage by adsorbed oxygen on the kinetics of oxygen reduction at oxide free platinum, Electrochimica Acta 18 (1973) 945.
[13] U. Krewer, T. Vidaković-Koch, L. Rihko-Struckmann, Electrochemical oxidation of carbon-containing fuels and their dynamics in low-temperature fuel cells, ChemPhysChem 12 (2011) 2518.
[14] U. Krewer, H.K. Yoon, H.T. Kim, Basic model for membrane electrode assembly design for direct methanol fuel cells, Journal of Power Sources 175 (2008) 760.
[15] Q. Mao, U. Krewer, R. Hanke-Rauschenbach, Total harmonic distortion analysis for direct methanol fuel cell anode, Electrochemistry Communications 12 (2010) 1517.
[16] T. Kadyk, R. Hanke-Rauschenbach, K. Sundmacher, Nonlinear frequency response analysis of PEM fuel cells for diagnosis of dehydration, flooding and CO-poisoning, Journal of Electroanalytical Chemistry 630 (2009) 19.
[17] T.R. Vidaković-Koch, V.V. Panić, Milan Andrić, K. Menka Petkovska, Sundmacher, Nonlinear frequency response analysis of the ferrocyanide oxidation kinetics. Part I. A theoretical analysis, Journal of Physical Chemistry C 115 (2011) 17341.
[18] V.V. Panić, T.R. Vidaković-Koch, Milan Andrić, K. Menka Petkovska, Sundmacher, Nonlinear frequency response analysis of the ferrocyanide oxidation kinetics. Part II. Measurement routine and experimental validation, Journal of Physical Chemistry C 115 (2011) 17352.
[19] J.R. Wilson, M. Sase, T. Kawada, S.B. Adler, Measurement of oxygen exchange kinetics on thin-film $La_{0.6}Sr_{0.4}CoO_{3-\delta}$ using nonlinear electrochemical impedance spectroscopy, Electrochemical and Solid-State Letters 10 (2007) B81.
[20] B. Bensmann, M. Petkovska, T. Vidakovic-Koch, R. Hanke-Rauschenbach, K. Sundmacher, Nonlinear frequency response of electrochemical methanol oxidation kinetics: a theoretical analysis, Journal of the Electrochemical Society 157 (2010) B1279.
[21] T. Kadyk, R. Hanke-Rauschenbach, K. Sundmacher, Nonlinear frequency response analysis for the diagnosis of carbon monoxide poisoning in PEM fuel cell anodes, Journal of Applied Electrochemistry 41 (2011) 1021.
[22] T. Kadyk, R. Hanke-Rauschenbach, K. Sundmacher, Nonlinear frequency response analysis of dehydration phenomena in polymer electrolyte membrane fuel cells, International Journal of Hydrogen Energy 37 (2012) 7689.
[23] Q. Mao, U. Krewer, Sensing methanol concentration in direct methanol fuel cell with total harmonic distortion: theory and application, Electrochimica Acta 68 (2012) 60.
[24] E. Ramschak, Method for monitoring the operational state of a fuel cell stack, US2006/0078788A1.
[25] T. Schaffer, W.R. Baumgartner, E. Wallnöfer, V. Hacker, E. Ramschak, V. Peinecke, P. Prenninger, Detection of critical operating conditions for fuel cell applications via distortion analysis, Meeting Abstracts (Electrochemical Society) 602 (2006) 428.
[26] U. Krewer, A. Kamat, K. Sundmacher, Understanding the dynamic behaviour of direct methanol fuel cells: Response to step changes in cell current, Journal of Electroanalytical Chemistry 609 (2007) 105.
[27] U. Krewer, M. Pfafferodt, A. Kamat, D. Fernandez Menendez, K. Sundmacher, Hydrodynamic characterisation and modelling of anode flow fields of direct methanol fuel cells, Chemical Engineering Journal 126 (2007) 87.
[28] J. Newman, E. Karen, Thomas-Alyea, Electrochemical Systems, 3rd ed., Wiley John & Sons, Yew York, 2004.
[29] Q. Mao, U. Krewer, R. Hanke-Rauschenbach, Total harmonic distortion analysis for direct methanol fuel cell anode, in: 61st Annual Meeting of the International Society of Electrochemistry, Nice, France, 26 September–1 October, 2010.

[30] J.-M. Le Canut, R.M. Abouatallah, D.A. Harrington, Detection of membrane drying, fuel cell flooding, and anode catalyst poisoning on PEMFC stacks by electrochemical impedance spectroscopy, Journal of the Electrochemical Society 153 (2006) A857.
[31] M.C. Tavares, S.A.S. Machado, L.H. Mazo, Study of hydrogen evolution reaction in acid medium on Pt micro electrodes, Electrochimica Acta 46 (2001) 4359.
[32] B.E. Conway, L. Bai, Determination of adsorption of OPD H species in the cathodic hydrogen evolution reaction at Pt in relation to electrocatalysis, Journal of Electroanalytical Chemistry 198 (1986) 149.
[33] E.N. Fuller, P.D. Schettler, J.C. Giddings, A new method for prediction of binary gas-phase diffusion coefficients, Industrial and Engineering Chemistry 58 (1966) 19.